Hirosaki Med. J. 66 : 152—161, 2016

ORIGINAL ARTICLE

IMAGE PROCESSING METHOD FOR VISUALIZING WHITE ZONE IN MAGNIFYING ENDOSCOPY WITH NARROW-BAND IMAGING OF GASTRIC MUCOSA.

Kenta Yoshida[1)], Yoshihiro Sasaki[2)], Norihiro Hanabata[1)], Tatsuya Mikami[1)], Hiroshi Kijima[3)] and Shinsaku Fukuda[1)]

Abstract White zone visualized by magnifying endoscopy with narrow-band imaging (M-NBI) corresponds to stratified alignments of the gastric epithelium. In this study, we develop an image processing method for white zone with high sensitivity. Eleven specimens of endoscopic submucosal resection from 8 patients with gastric cancer were used. M-NBI was taken serially along the line of interest. The pictures were processed by low-pass filter for white zone area (%), and visually classified into the presence (WZ+) or absence of white zone (WZ−) by a single endoscopist. The formalin-fixed-specimen was sliced along the same line of interest. The histological pictures was processed for averaged epithelial area (μm×mm) at 1mm intervals. A total of 123 intervals were analyzed. In cancer, 36 intervals were visually classified as WZ- and 30 as WZ+. Averaged epithelial area and white zone area were significantly lower in WZ− than in WZ+. But, in background, two variables did not significantly differ between WZ− and WZ+. A total of 117 intervals had averaged epithelial area > 20 μm×mm and white zone area > 21.0 % with no correlation between two variables. Low-pass filter was found to visualize white zone in 41 intervals classified as WZ−.

Hirosaki Med. J. 66 : 152—161, 2016

Key words: Magnifying endoscopy; Narrow-band imaging; Early gastric cancer; White zone; Image processing.

Introduction

With the advent of magnifying endoscopy, it has become possible to visualize microvessels less than 10μm in size against the background. The microvascular architecture has been employed for characterizing early gastric cancer[1-3)] or gastritis with positive Helicobacter Pylori (*H Pylori*) [4, 5)]. Magnifying endoscopy with narrow-band imaging (M-NBI) has markedly enhanced the microvascular area compared with white light endoscopy.[6)] In the enhanced image, the microvessels can be traced as a low reflectance area against the background with a high contrast. We have developed an image processing method for microvessel segmentation and demonstrated significant differences in the microvessel morphological variables between cancer and the surrounding background in gastric mucosa[7)].

Another striking achievement of M-NBI has visualized microsurface pattern resulting from the different scattering properties[6)]. Microsurface pattern or white zone is recognized as pale brownish stripes, which has been reported to correspond to the stratified arrangements of the marginal crypt epithelium[8, 9)]. The aims of this study were to develop an image processing method for white zone area and correlate with histological epithelial area in two visually evaluated categories (the presence or absence of white zone).

Department of [1)] Gastroenterology and [2)]Medical Informatics, Hirosaki University Hospital, [3)]Pathology and Bioscience, Hirosaki University Graduate School of Medicine, 53 Hon-cho, Hirosaki, 036-8563, Japan.

Correspondence: Y. Sasaki
Received for publication, November 26, 2015
Accepted for publication, December 8, 2015

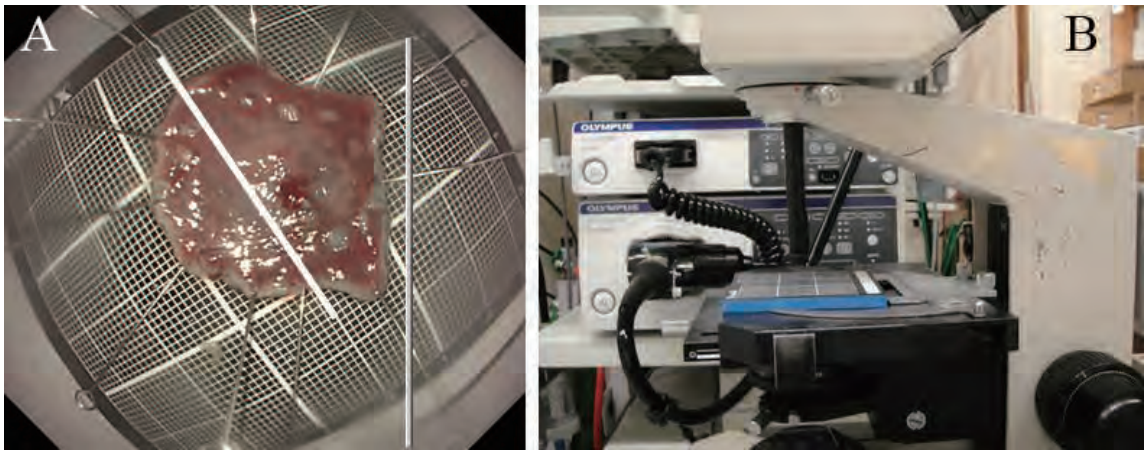

Figure 1 (A) Specimen of endoscopic submucosal resection for early gastric cancer fixed on the graph panel. The pictures were taken at the maximal magnification with structural intensification of A8 along the line of interest (white line). The specimen was fixed in 10% neutral buffered formalin and sliced along the same line of interest for histological analysis. (B) The panel was topographically manipulated on the stage of microscope together with endoscope fixed in the lens-barrel.

Methods

Materials

Eleven specimens of endoscopic submucosal resection from 8 male patients with gastric cancer (mean age, 75.2 years old) were used. M-NBI was taken serially along the line of interest placed in the specimen fixed on graph panel (Figure 1A). The panel was topographically manipulated on the stage of microscope together with endoscope fixed in the lens-barrel (Figure 1B). The pictures were taken in the direction perpendicular to the specimen's surface at the maximal magnification with structural intensification of A8 (Lucera 290 for a control unit and GIF-H260Z for an endoscope, Olympus, Tokyo, Japan), and saved in a digital filing system with the size of 1000X870 pixels (IN10J, Olympus, Tokyo, Japan). The specimen was fixed in 10% neutral buffered formalin and sliced along the same line of interest for histological analysis (H&E staining). Ethics clearance for this research was provided by the Ethics Committee of Hirosaki University Graduate School of Medicine at April 24th, 2015 (permission number: 2014-361).

Correction of barrel distortion

Endoscopic images inherently suffer from barrel distortion because of the fish eye lens (Figure 2-A). In the distorted image, magnification decreases as a distance from the image center increases. By using polynominal distortion model[10], the distorted image was transformed to the undistorted one, where parallel straight lines are represented. In the process, the margin of the transformed picture was trimmed because of distortion remaining (Figure 2-B). Spatial resolution was found to be 3mm /940 pixels or 3.19 μm /pixel at the maximal magnification.

White zone in narrow-band imaging

In M-NBI, green (540 to 570 nm) and blue narrow-band light (420 to 450 nm) are irradiated on the surface of the mucosa. A single narrow-band imaging picture is composed of the green reflectance (assigned to red color channel) and blue reflectance (assigned to green and blue color channels) images (Figure 3-A). As the intensity of backward scattering decreases along with the wavelengths[11], blue lights travel to

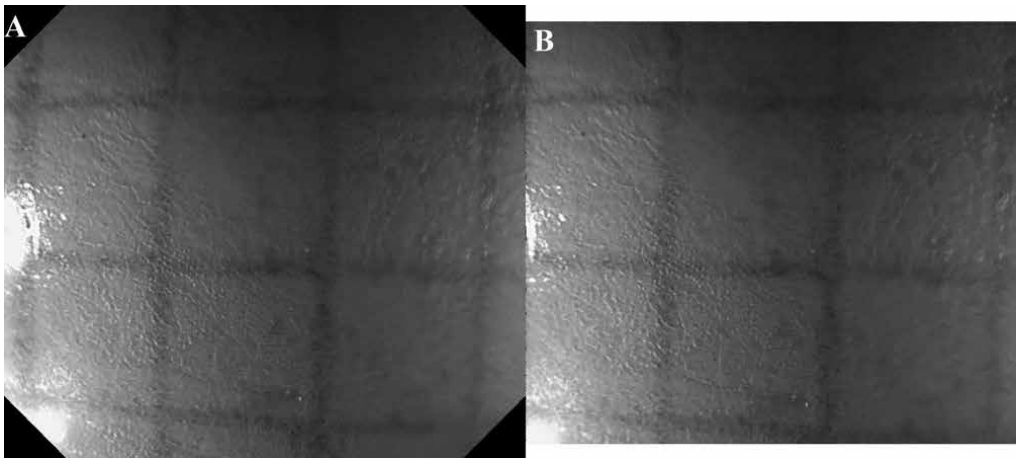

Figure 2 (A) The magnifying endoscopic picture of a squared paper (the line interval of 1mm). The straight lines suffer from barrel distortion because of the fish eye lens. (B) The undistorted picture of the panel A by using polynominal distortion model, where the margin of the transformed picture was trimmed because of distortion remaining. The straight lines of the squared paper are represented. Spatial resolution was found to be 3.19 μm /pixel at the maximal magnification.

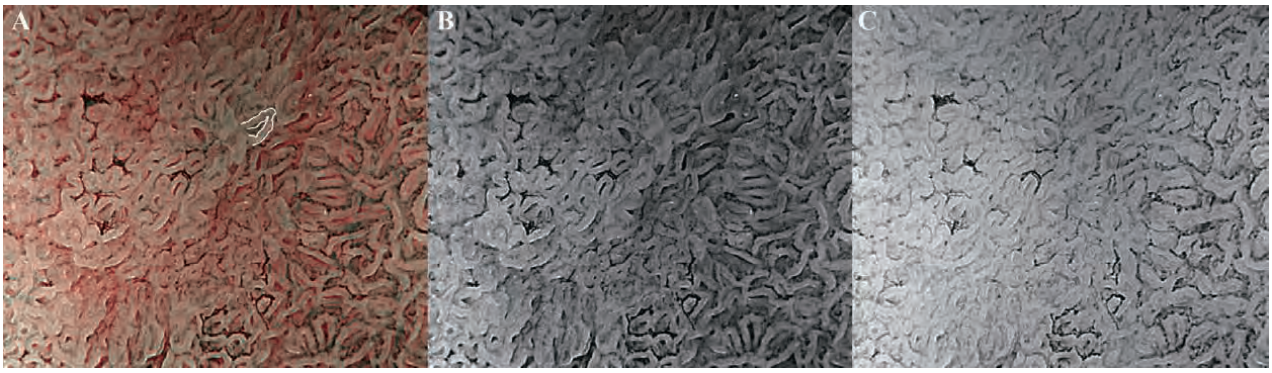

Figure 3 White zone in narrow-band imaging. (A) M-NBI of the gastric antrum (3.19 μm /pixel). White zone is recognized as pale brownish stripes (the border of white zone was marked by the white lines). Details described in reference 8). (B) The blue reflectance (420 to 450 nm) composing the original picture A. White zone was clearly traced with high contrast. (C) The green reflectance (540 to 570 nm) composing the original picture A with low-contrast white zone.

become faint in the shallow part of the gastric tissue, while green lights to reach the deeper part.

As white zone has been reported to correspond to the stratified arrangements of columnar cells which cover the gastric pits [8, 9], it is visualized with a higher contrast in the blue reflectance (green color channel) than in the green reflectance (red color channel) (Figure 3-B and C, respectively).

White zone segmentation

When the blue reflectance (Figure 3-B) was processed by frequency filter [12] with a low-pass band of less than Nyquist × 0.1, the picture with enhanced white zone and microvessel eliminated was obtained (Figure 4A). The topographic intensity of the processed picture was shown in Figure 4B, where white zone was geographically represented as the ridges. The curvature of the ridges was reasonably quantified by Laplacian operator.[13] Let the reflectance intensity with

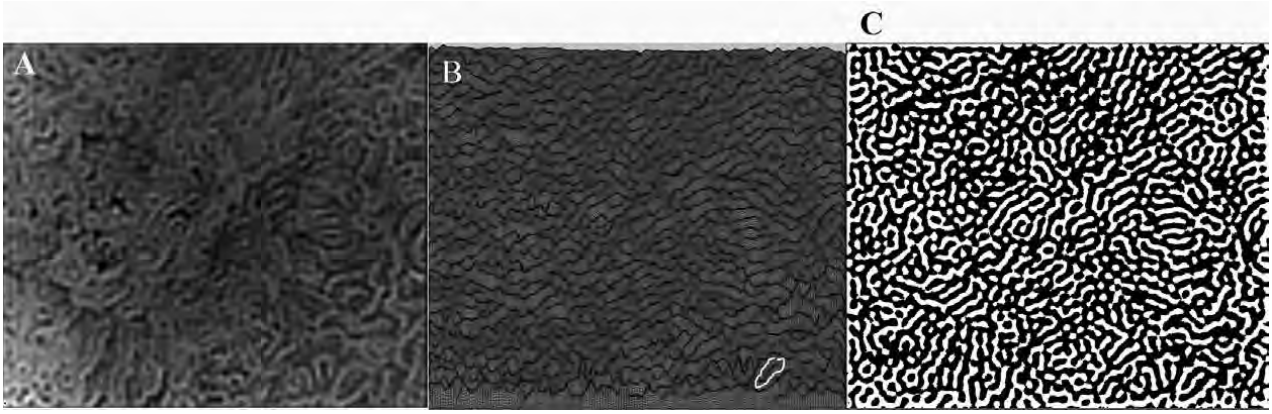

Figure 4 White zone segmentation. (A) Picture obtained from Figure 3B through frequency filter with a low-pass band of less than Nyquist×0.1, where white zone was enhanced and microvessels were eliminated. (B) The topographic intensity of the panel A. White zone was geographically represented as the ridges, which is defined as the upper projection part with a larger curvature of the topographical map (white line). (C) The ridges were reasonably segmented by Laplacian operator. The segmented white zone was automatically calculated for white zone area against the region of interest (%).

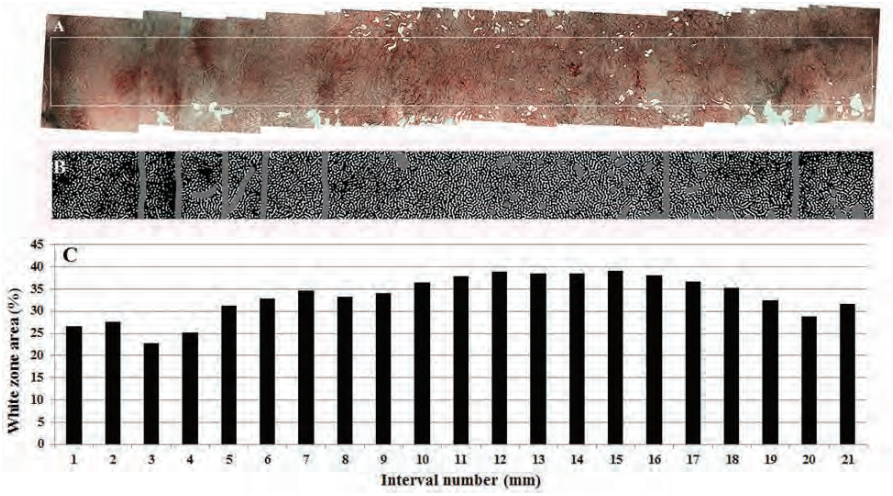

Figure 5 (A) M-NBI taken serially along the line of interest on the resected specimen was manually joined so that they fit together (3.19 μm / pixel). (B) Segmented white zone (white area) in the region of interest with 21.7 mm length and 1.8 mm height (white rectangle in the panel A). (C) By using image processing, white zone area (%) was calculated at every 1mm lateral intervals along the region of interest.

low-pass filter at picture coordinates (x, y) I (x,y). A Laplacian value at (x,y) is given by the sum of I(x+i, y+j) − I(x,y) for i= −1, 0, 1 and j= −1, 0, 1. When Laplacian at (x,y) < −1, the point was considered as a point composing white zone (Figure 4C). The segmented white zone was automatically calculated for the % ratio of white zone against the region of interest (white zone area).

White zone area along the sliced line

M-NBI taken serially along the line of interest on the resected specimen was manually joined so that they fit together (Figure 5A). The serial picture was visually classified into the presence (WZ+) or absence of white zone (WZ−) at 1mm lateral intervals by a single experienced endoscopist (T.M.). Figure 5B designates

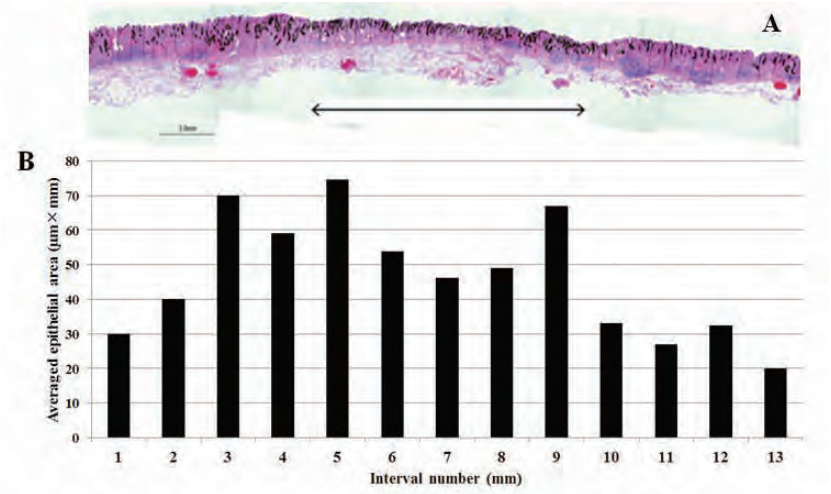

Figure 6 (A) The histological pictures with magnification of 40 taken serially along the sliced line corresponding to endoscopic analysis (Figure 5A) were manually joined so that they fit together. The region of interest includes cancer (the two-way arrow) and background area. The black line in the lower left designates 1mm scale length. Area of epithelium was manually painted in black. (B) By using image processing, averaged epithelial area (μm × mm) was calculated at every 1mm lateral intervals, where parts affected by burning effect at both ends of the specimen or by mechanical injuries were excluded from analysis.

segmented white zone (white area) in the region of interest with 21.7 mm length and 1.8 mm height (white rectangle in Figure 5A), where halation, joint lines neighboring pictures and out of focus area were excluded from analysis. White zone area (%) was calculated at every 1mm intervals along the region of interest (Figure 5C).

Histological analysis

The histological pictures with magnification of 40 taken serially along the sliced line corresponding to endoscopic analysis (Figure 5A) were manually joined so that they fit together, and the epithelium was manually painted in black (Figure 6A). Averaged epithelial area (μm × mm) was calculated at every 1mm lateral intervals (Figure 6B), where parts affected by burning effect at both ends of the specimen or by mechanical injuries were excluded from the analysis.

Statistics

All variables are expressed by the mean ± SD. Correlation coefficient between white zone area and averaged epithelial area was used by Pearson's method. All tests were carried out two-tailed t-test with a significance level of 5% by using Microsoft Excel 2010.

Results

Macroscopic and histological findings

The macroscopic types of gastric cancer were classified into IIa (5) and IIc (6) [14]. Six lesions were identified in the gastric body and the remaining 5 ones in the antrum. The maximal diameter of the lesions ranged 8 mm to 42 mm (the mean size of 23.9 mm). The histology of the ESD specimen was classified into well differentiated adenocarcinoma (8) and moderately differentiated adenocarcinoma (3).

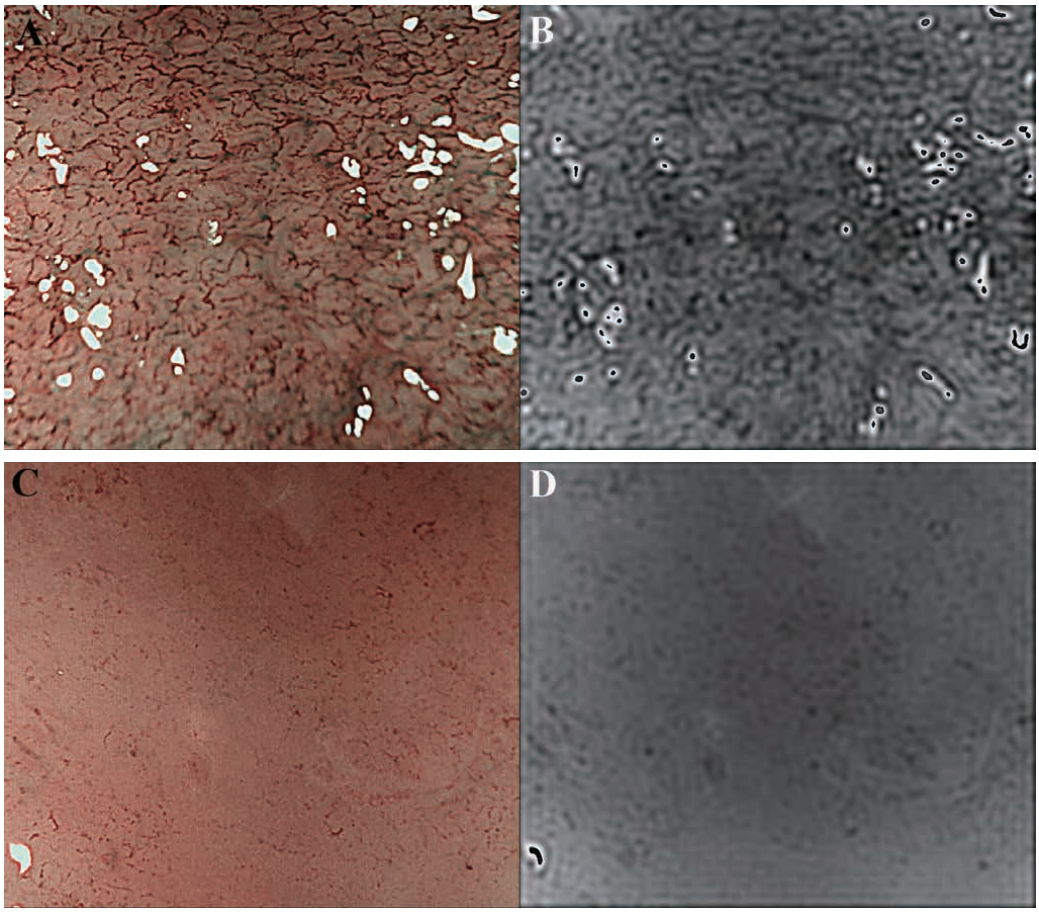

Figure 7 Pairs of M-NBI visually classified as the absence of white zone and the corresponding processed picture. (A) 0-IIb lesion in the gastric body with averaged epithelial area of 81.9 μm×mm. (B) Processed picture of the panel A with white zone area of 38.6 %. (C) Poorly differentiated part of 0-IIa lesion in the gastric body with averaged epithelial area of 1.1 μm×mm. (D) Processed picture of the panel C with a minimal white zone area of 7.3 %.

Ten lesions were confined to the mucosa or muscularis mucosae and 1 lesion was found to invade to the depth of the submucosa (400μm) without lymphatic and venous invasion.

Examples of low-pass filter processing

Pairs of M-NBI visually classified as WZ− and the corresponding processed picture were shown in Figure 7. Figure 7A was 0-IIb lesion in the gastric body with averaged epithelial area of 81.9 μm×mm. Low-pass filter processing visualized white zone area of 38.6 % (Figure 7B). Figure 7C was the poorly differentiated part of 0-IIa lesion in the gastric body with averaged epithelial area of 1.1 μm×mm. Under the absence of crypt epithelium, segmented white zone area was found to be a minimal value of 7.3 % (Figure 7D).

White zone area vs. averaged epithelial area

White zone area was plotted against averaged epithelial area in cancer (Figure 8A) and in background (Figure 8B). In cancer, 36 lateral intervals were visually classified as WZ− (open circle) and 30 as WZ+ (filled circle). Six intervals had no crypt area (1.8±2.8 μm×mm) with a minimal white zone area of 7.5±2.3%, where corresponds to poorly differentiated parts of cancer. The remaining 60 intervals had averaged epithelial area > 20 μm×mm and white zone area ranging 21.0 to 41.6 (32.7±5.0%), where

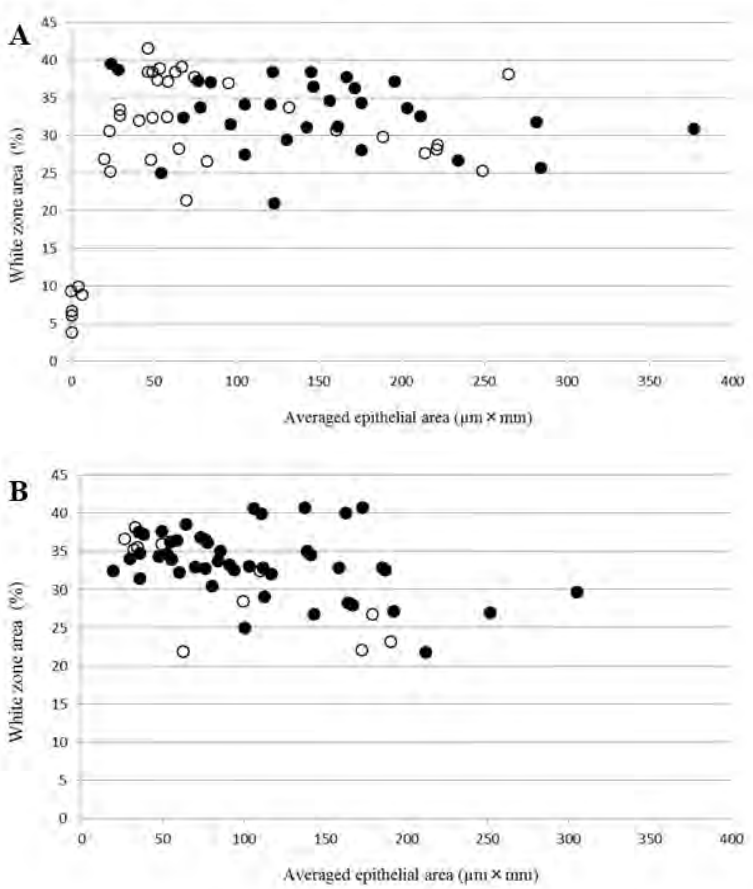

Figure 8 (A) White zone area (%) vs. averaged epithelial area (μm × mm) in cancer. Thirty six lateral intervals were visually classified as WZ- (open circle) and 30 as WZ+ (filled circle). Six intervals had no crypt area (1.8 ± 2.8 μm × mm) with a minimal white zone area of 7.5 ± 2.3%. The remaining 60 intervals had averaged epithelial area > 20 μm × mm and white zone area ranging 21.0 to 41.6 (32.7 ± 5.0%), where there was not any correlation between two variables (r= −0.209, p< 0.002). White zone area was significantly lower in WZ- (28.4 ± 10.7%) than in WZ+ (32.9 ± 4.6, p=0.0126%). Averaged epithelial area was also significantly lower in WZ- (77.9 ± 76.2 μm × mm) than in WZ+ (148.1 ± 77.8 μm × mm, p=0.0002). (B) White zone area (%) vs. averaged epithelial area (μm × mm) in background. Eleven intervals were visually classified as WZ- (open circle) and 46 as WZ+ (filled circle). All of 57 intervals had averaged epithelial area > 20 μm × mm and white zone ranging 21.7 to 40.8 (33.0 ± 4.8%) with no correlation between two variables (r= −0.442, p< 0.001). White zone area did not significantly differ between WZ- (30.5 ± 6.3%) and WZ+ (33.5 ± 4.3%, p=0.2508). Averaged epithelial area also did not significantly differ between WZ- (90.0 ± 64.3μm × mm) and WZ+ (107.2 ± 62.3 μm × mm, p= 0.2093).

there was not any correlation between two variables (r= −0.209, p< 0.002). White zone area was significantly lower in WZ- (28.4 ± 10.7%) than in WZ+ (32.9 ± 4.6%, p=0.0126). Averaged epithelial area was also significantly lower in WZ- (77.9 ± 76.2 μm × mm) than in WZ+ (148.1 ± 77.8 μm × mm, p=0.0002). In background, 11 intervals were visually classified as WZ- (open circle) and 46 as WZ+ (filled circle). All of 57 intervals had averaged epithelial area > 20 μm × mm and white zone area ranging from 21.7 to 40.8 (33.0 ± 4.8%) with no correlation between two variables (r= −0.442, p< 0.001). White zone area did not significantly differ between WZ- (30.5 ± 6.3%) and WZ+ (33.5 ± 4.3%, p=0.2508). Averaged epithelial area also did not significantly differ between WZ- (90.0 ± 64.3 μm × mm) and WZ+ (107.2 ± 62.3 μm × mm, p= 0.2093). These findings have indicated that when averaged epithelial area exceeds 20 μm × mm, low-pass

filter processing can visualize white zone even in the intervals visually classified as WZ− (30 intervals in cancer and 11 in background).

Discussion

The current study has correlated endoscopic white zone area with histological epithelial area in two categories visually classified as the presence or absence of white zone. Demonstrated was that (1) white zone area was found < 10 % under averaged epithelial area < 10 μm×mm, (2) white zone area was >21.0 % under averaged epithelial area > 20 μm×mm without significant correlation between two variables, (3) low-pass filter processing has visualized white zone in 41 intervals visually classified as the absence of white zone.

M-NBI has markedly enhanced the microvascular area and microsurface pattern compared with white light magnifying endoscopy. The new diagnostic modality has led to the diagnostic system for early gastric cancer[9, 15]. We have previously developed an image processing method for microvessel segmentation and demonstrated significant differences in the microvessel morphology between cancer and the surrounding background in gastric mucosa[7]. Microsurface pattern or white zone is recognized as pale brownish stripes, which can be optically defined as an area with higher reflectance intensity. We have noticed that white zone has been effectively extracted by using low-pass filter even in a case with poor visual discrimination. In this study, low-pass filter processing has been demonstrated to segment white zone visually classified as the absence of white zone with high sensitivity, leading to differentiation between the presence or absence of crypt alignments.

Conventional comparative studies between endoscopic and histological variables have been conducted by using biopsy specimens. This method has been considered to suffer from a limited number of samples or limited reliability for mapping. In this study, ESD specimens mounted on the stage of microscope together with endoscope fixed in the lens-barrel was used for precise picture acquisition along the section line for histological analysis. This has enabled a point to point correlation analysis between endoscopic and histologic variables.

In the present study, white zone area has not been correlated with averaged epithelial area when averaged epithelial area exceeds 20 μm×mm. This suggests that other histological variables may be involved in white zone synthesis. Optical scattering properties of individual epithelial cells have been considered to be one of factors for explanation. The presence of chronic inflammation, for example, brush border or goblet cells can enhance backward scattering [16], which has led to higher white zone area. Short intervening part and/or short crypt [8] can make white zone discrimination obscure. For more understanding of white zone, the features of individual cells and crypt arrangements have to be taken in account as well as averaged epithelial area.

We have previously reported a reliable image processing method to extract the morphological features for spatial arrangements of mucosal color[17], the degree of mucosal surface roughness[18] and micro vasculatures[7]. A variety of endoscopic features in magnifying endoscopy with NBI has been reported as a clue to differentiation between early gastric cancer and low grade adenoma[19, 20], a marker for the diagnosis of papillary adenocarcinoma[21] and early gastric cancer of undifferentiated type[22]. When quantitative method for these endoscopic features is developed, it may provide endoscopists with potential tools to improve reliability in image interpretation by minimizing inter-observer variation. The challenge is now to characterize cancer area or the demarcation line for auto-segmentation of early gastric cancer by more

integrated pattern classification method.

References

1) Yao K, Oishi T, Matui T, Mathui T, Tao T, Iwashita A. Novel magnified endoscopic findings of microvascular architecture in intramucosal gastric cancer. Gastrointest Endosc. 2002;56:278-84.

2) Tajiri H, Doi T, Endo H, Nishina T, Terao T, Hyodo I, Matsuda K, et al. Routine endoscopy using a magnifying endoscope for gastric cancer diagnosis. Endoscopy. 2001;34:772-7.

3) Otsuka Y, Niwa Y, Ohmiya N, Ando N, Ohashi A, Hirooka Y, Goto H. Usefulness of magnifying endoscopy in the diagnosis of early gastric cancer. Endoscopy. 2004;36:165-9.

4) Yagi K, Nakamura A, Sekine A. Comparison between magnifying endoscopy and histological, culture and urease test findings from the gastric mucosa of the corpus. Endoscopy. 2002;34:376-81.

5) Nakagawa S, Kato M, Shimizu Y, Nakagawa M, Yamamoto J, Perez AL, Kodaira J, et al. Relationship between histopathologic gastritis and mucosal microvascularity: observations with magnifying endoscopy. Gastrointest Endosc. 2003;58:71-5.

6) Yao K, Takaki Y, Matsui T, Iwashita A, George K, Philip K, Krish R. Clinical application of magnification endoscopy and narrow-band imaging in the upper gastrointestinal tract: New imaging techniques for detecting and characterizing gastrointestinal neoplasia. Gastrointest Endosc Clin N Am. 2008;18:415-33.

7) Araki Y, Sasaki Y, Hanabata N, Yoshimura T, Sawaya M, Hada R, Fukuda S. Morphometry for microvessels in early gastric cancer by narrow band imaging- equipped magnifying endoscopy. Digestive Endosc. 2011;23:233-9.

8) Yagi K, Nozawa Y, Endou S, Nakamura A. Diagnosis of early gastric cancer by magnifying endoscopy with NBI from viewpoint of histological imaging: mucosal patterning in terms of white zone visibility and its relationship to histology. Diag Therap Endosc. Published online. 2012[DOI:10.1155/2012/954809].

9) Yao K. The endoscopic diagnosis of early gastric cancer. Ann Gastroenterol. 2013;26:11–22.

10) Devernay F, Faugeras O. Straight lines have to be straight. Automatic calibration and removal of distortion from scenes of structured environments. Mach Vis Appl. 2001;13:14–24.

11) Bohren CF, Huffman DR. Particles small compared with the wavelength. In: Bohren CF, Huffman DR, eds. Absorption and Scattering of light by small particles. New York: John Wiley & sons; 1998. p.130-6.

12) Seul M, O'Gorman L, Sammon MJ. Practical algorithms for image analysis. Description, examples, and code. Cambridge: Cambridge University Press; 2000. p.247-72.

13) Parker JR. Algorithms for image processing and computer vision. New York: John Wiley & Sons; 1997. p.21-2.

14) Japanese Gastric Cancer Association. Japanese classification of gastric carcinoma. 3rd English edition. Gastric Cancer. 2011;14:101-112.

15) Yao K, Anagnostopoulos GK, Ragunath K. Magnifying endoscopy for diagnosis and delineating early gastric cancer. Endoscopy. 2009;41:462-8.

16) Uedo N, Ishihara R, Iishi H, Yamamoto S, Yamamoto S, Yamada T, Imanaka K et al. A new method of diagnosing gastric intestinal metaplasia: narrow-band imaging with magnifying endoscopy. Endoscopy. 2006;38:819-24.

17) Sasaki Y, Hada R, Munakata A. Computer-aided grading system for endoscopic severity in patients with ulcerative colitis. Dig Endosc. 2003;15:206-9.

18) Sasaki Y, Fukuda S, Mikami T, Hada R . Endoscopic quantification of mucosal surface roughness for grading severity of ulcerative colitis. Dig Endosc. 2008;20:67-72.

19) Doyama H, Yoshida N, Tsuyama S, Ota R, Takeda Y, Nakanishi H, Tsuji K, et al. The "white globe appearance" (WGA): a novel marker for a correct diagnosis of early gastric cancer by magnifying endoscopy with narrow-band imaging (M-NBI). Endosc Int Open. 2015;03:E120-4.

20) Kanesaka T, Sekikawa A, Tsumura T, Maruo T, Osaki Y, Wakasa T, Shintaku M, et al. Dense-type crypt opening seen on magnifying endoscopy with narrow-band imaging is a feature of gastric adenoma. Dig Endosc. 2014;26:57-62.

21) Kanemitsu T, Yao K, Nagahama T, Fujiwara S, Takaki Y, Ono Y, Matsushima Y, et al. The vessels within epithelial circle (VEC) pattern as visualized by magnifying endoscopy with narrow-band imaging (ME-NBI) is a useful marker for the diagnosis of papillary adenocarcinoma: a case-controlled study. Gastric Cancer. 2014;17:469-77.

22) Kanesaka T, Sekikawa A, Tsumura T, Maruo T, Osaki Y, Wakasa T, Shintaku M, et al. Absent microsurface pattern is characteristic of early gastric cancer of undifferentiated type: magnifying endoscopy with narrow-band imaging. Gastrointest Endosc. 2014;80:1194-8.